



HAL
open science

Diving into the brain: deep-brain imaging techniques in conscious animals

Pauline Campos, Jamie Walker, Patrice Mollard

► **To cite this version:**

Pauline Campos, Jamie Walker, Patrice Mollard. Diving into the brain: deep-brain imaging techniques in conscious animals. *Journal of Endocrinology*, 2020, 10.1530/JOE-20-0028 . hal-02863790

HAL Id: hal-02863790

<https://hal.science/hal-02863790>

Submitted on 17 Dec 2020

HAL is a multi-disciplinary open access archive for the deposit and dissemination of scientific research documents, whether they are published or not. The documents may come from teaching and research institutions in France or abroad, or from public or private research centers.

L'archive ouverte pluridisciplinaire **HAL**, est destinée au dépôt et à la diffusion de documents scientifiques de niveau recherche, publiés ou non, émanant des établissements d'enseignement et de recherche français ou étrangers, des laboratoires publics ou privés.

Diving into the brain: deep-brain imaging techniques in conscious animals

Pauline Campos¹, Jamie J. Walker^{1,2,3}, Patrice Mollard⁴

¹ College of Engineering, Mathematics and Physical Sciences, University of Exeter, Exeter, United-Kingdom

² EPSRC Centre for Predictive Modelling in Healthcare, University of Exeter, Exeter, United Kingdom

³ Bristol Medical School, Translational Health Sciences, University of Bristol, Bristol, United Kingdom

⁴ IGF, Univ. Montpellier, CNRS, INSERM, Montpellier, France

Corresponding author: Dr. Pauline Campos, College of University of Engineering, Mathematics and Physical Sciences, University of Exeter, Exeter EX4 4PS, United-Kingdom.

(phone: +44 7 484 838 763, email: p.campos@exeter.ac.uk)

Running Head: Deep-brain imaging techniques in conscious rodents.

Keywords: Neuroendocrinology, Whole animal physiology, Deep-brain imaging, Neuronal activity, Conscious animals

27
28
29
30
31
32
33
34
35
36
37
38
39
40
41
42
43
44
45
46
47
48
49
50
51
52
53
54
55
56

In most species, survival relies on the hypothalamic control of endocrine axes that regulate critical functions such as reproduction, growth, and metabolism. For decades, the complexity and inaccessibility of the hypothalamic-pituitary axis has prevented researchers from elucidating the relationship between the activity of endocrine hypothalamic neurons and pituitary hormone secretion. Indeed, the study of central control of endocrine function has been largely dominated by ‘traditional’ techniques that consist of studying *in vitro* or *ex vivo* isolated cell types without taking into account the complexity of regulatory mechanisms at the level of the brain, pituitary and periphery. Nowadays, by exploiting modern neuronal transfection and imaging techniques, it is possible to study hypothalamic neuron activity *in situ*, in real time, and in conscious animals. Deep-brain imaging of calcium activity can be performed through gradient-index lenses that are chronically implanted and offer a ‘window into the brain’ to image multiple neurons at single-cell resolution. With this review, we aim to highlight deep-brain imaging techniques that enable the study of neuroendocrine neurons in awake animals whilst maintaining the integrity of regulatory loops between the brain, pituitary and peripheral glands. Furthermore, to assist researchers in setting up these techniques, we discuss the equipment required, and include a practical step-by-step guide to performing these deep-brain imaging studies.

57
58
59
60
61
62
63
64
65
66
67
68
69
70
71
72
73

For almost a century, neuroendocrinologists have worked towards characterising the central regulation of endocrine axes that ensure critical functions such as reproduction, growth, and metabolism. While research questions have for many years focused firmly on the neural control of the pituitary gland, the neuroendocrinology field has grown wider and now includes studying the effect of centrally-produced hormones on various brain areas, as well as the role of several peripherally-born peptides that affect neuroendocrine systems controlling metabolism. An unavoidable feature of all neuroendocrine systems is that they generate rhythms and rely on these rhythms to function optimally. These hormone oscillations dynamically regulate gene transcription and synaptic transmission, and changes in these oscillations are observed in a variety of (patho)physiological states (Le Tissier et al., 2017).

74
75
76
77
78
79
80
81
82
83
84
85
86
87
88
89

Although it has long been postulated that neuroendocrine neurons have the ability to generate hormone rhythms via the patterning of their electrophysiological activity, the regulatory mechanisms underlying this rhythmic mode of hormone secretion have remained hazy. One reason for this is that research efforts in this area have simply been hindered by the complexity and inaccessibility of the hypothalamic-pituitary system. Another reason is that the study of neuroendocrine function has been largely dominated by techniques that consist of studying isolated cell types in *in vitro* or *ex vivo* preparations. This insular approach has led to an inevitable bottleneck where data on cellular and biochemical processes within specific cell types or nuclei have multiplied without a clear/tangible link to physiological function. Similarly, recent efforts in single-cell transcriptomics of the hypothalamus (Romanov et al., 2017; Wang and Ma, 2019) have documented a highly complex heterogenous hypothalamus, but the implication of neuropeptide expression for physiological function remains difficult to interpret without appropriate tools. Nevertheless, technological developments in genetics and systems neuroscience have enabled specific neurons to be manipulated *in vivo*. Chemogenetics and optogenetics (Fenno et al., 2011) tools have made it possible to study the hypothalamus in ways that were previously unimaginable, shedding light on gonadotropin pulse generation (Campos and Herbison, 2014; Han et al., 2015; Voliotis et al., 2019) and brain control of appetite for example (Atasoy et al.,

90 2012; Betley et al., 2015). Likewise, genetically-encoded calcium indicators (GECIs) (Pérez
91 Koldenkova and Nagai, 2013) are now frequently used to monitor neuronal activity in living animals.
92 Their characteristics making them an excellent proxy for electrical activity and a versatile tool that
93 facilitates diverse imaging techniques. For example, fibre photometry experiments that consist of
94 monitoring the average calcium activity of a neuronal population *in vivo* have shown that arcuate
95 kisspeptin neurons are responsible for the generation of pulses of LH (Clarkson et al., 2017).

96 Despite the valuable insights these techniques have provided, none of them have allowed
97 researchers to study neuronal activity across a population at the single-cell level—characterising for
98 example cell-to-cell heterogeneity or synchronicity—and in turn relate this activity to specific
99 functions. Fortunately, deep-brain single-cell imaging can now be achieved using gradient-index
100 (GRIN) lenses that are chronically implanted and permit imaging of multiple (10-100s) neurons within
101 the population (Barretto et al., 2009). Depending on the research question and image quality required,
102 visualisation of neuronal activity can be carried out in head-fixed configuration using a bench-top
103 microscope (Bocarsly et al., 2015; Kim et al., 2010, 2009), or in freely-moving configuration using a
104 miniature head-mounted microscope (Ghosh et al., 2011). Importantly, using these techniques, it
105 becomes possible to correlate the impact of neuronal activity within a network on other functions. This
106 methodology has been successfully used to study arcuate nucleus and amygdala control of feeding
107 behaviour in freely-moving mice (Betley et al., 2015; Jennings et al., 2015). Similarly, head-fixed
108 microscopy through GRIN lenses has made possible to image and manipulate pituitary cells over a
109 period of days to weeks in awake mice (Hoa et al., 2019) and while it has yet to be published, one can
110 easily imagine combining this technique with serial blood sampling to understand the link between the
111 activity of specific hypothalamic neurons and the resulting peripheral hormonal release (Fig1). In the
112 near future, *in vivo* deep-brain imaging could become critical when combined with other emerging
113 strategies. For example, researchers now have the ability to visualise *in vivo* the effect on neuronal
114 activity of individual genomic variants identified from human genomes, thus filling a gap in our general
115 view of neuroendocrine systems (Fig1).

116 In this review, we will discuss deep-brain imaging techniques that enable the study of
117 endogenous brain activity from neuroendocrine populations in awake animals whilst maintaining the
118 integrity of regulatory loops between the brain, pituitary and peripheral glands. Rather than cataloguing
119 all available methodologies, we will focus on the most widely used and accessible systems, and provide
120 advice on neuronal activity indicators, neuronal targeting, microscopy techniques, analysis, animal
121 handling and physiological/behavioural assessments so that researchers will be able to set up these
122 techniques to address their own research questions.

123

124 **1. Monitoring neuronal activity with genetically-encoded indicators**

125 In order to understand brain processing, scientists have tried to decrypt the action potential (AP) firing
126 of groups of neurons and relate this to specific physiological functions. Traditional methods such as
127 intracellular patch-clamp limit the number of neurons that can be studied at the same time, are invasive
128 and difficult to perform *in vivo*. Extracellular recordings are easier to make, but do not give precise
129 information about the electrical activity of individual neurons, and do not enable the study of specific
130 neuronal firing within a population. Looking to overcome these issues, Francis Crick proposed in 1999
131 that “One way-out suggestion is to engineer these neurons so that when one of them fires it would emit
132 a flash of light of a particular wave length” (Crick, 1999); and indeed, the development of genetically-
133 encoded optical indicators of neuronal activity has enabled progress toward this goal to an extent that
134 was unimaginable two decades ago. Nowadays, optical imaging enables thousands of neurons to be
135 simultaneously observed *in vitro* or *in vivo*, whilst voltage and calcium indicators reveal spatiotemporal
136 activity patterns within neurons such as dendritic integration, voltage propagation, or dendritic spiking
137 (Lin and Schnitzer, 2016). Although microscopy requires optical access to the tissue of interest, many
138 techniques allow minimally-invasive optical access or placement of optical probes up to millimetres
139 away from the imaged cells, thus allowing the immediate vicinity of cells under study to be left
140 unperturbed (Betley et al., 2015; Ghosh et al., 2011).

141

142 **a. Calcium indicators**

143 Calcium is a universal second messenger, playing an essential role in excitable cells and signal
144 transduction. In neurons, APs trigger large and rapid calcium (Ca^{2+}) influx through voltage-gated
145 channels. AP firing can therefore be assessed by measuring changes in concentrations of intracellular
146 Ca^{2+} (Yasuda et al., 2004). Similarly, activation of neurotransmitter receptors during synaptic
147 transmission causes Ca^{2+} transients in dendritic spines, and with appropriate indicators, imaging
148 intracellular Ca^{2+} dynamics can be used to measure neuronal spiking and synaptic activity across
149 populations of neurons *in vitro* and *in vivo*. GECIs and small-molecule calcium-sensitive dyes (Cobbold
150 and Rink, 1987) such as fura-2 (Grynkiewicz et al., 1985) are both used to report changes in intracellular
151 Ca^{2+} concentration; but GECIs have the advantage that they enable long term, repeated non-invasive
152 imaging of specific cells and compartments (Mao et al., 2008). State-of-the-art GECIs include Förster
153 Resonance Energy Transfer (FRET)-based sensors (Fiala et al., 2002; Mank et al., 2008; Palmer and
154 Tsien, 2006), but for *in vivo* experiments particularly, the single-wavelength sensor GCaMP family has
155 become the default tool (Tian et al., 2009). GCaMPs are based on circularly permuted green fluorescent
156 protein (cpGFP), calmodulin (CaM), and the Ca^{2+} /CaM-binding “M13” peptide. Ca^{2+} binding to the
157 calmodulin domain results in a structural shift that enhance the fluorescence by deprotonation of the
158 fluorophore. Since the original GCaMP sensor was published (Nakai et al., 2001), many variants have

159 been developed with the purpose of performing calcium imaging *in vivo* (Ohkura et al., 2005; Tallini et al., 2006; Tian et al., 2009). The experimenter will be burdened with picking the appropriate GECI from
160 a broad assortment, but generally-speaking, imaging from large populations of neurons in densely
161 labelled samples is helped by lower baseline fluorescence indicators, which reduces the background
162 signal from neuropil and inactive neurons (Dana et al., 2019). Moreover, low baseline fluorescence
163 becomes especially important when working *in vivo* where large tissue volumes contribute to the
164 background signal. For the reasons mentioned above, we and others have worked with GCaMP6s,m,f³¹
165 and are now experimenting with JGCaMP7f (Chen et al., 2013); all offer high signal-to-noise ratio
166 (SNR) and GCaMP6m and JGCaMP7 show improved detection of individual spikes (Chen et al., 2013;
167 Dana et al., 2019). It is also worth noting the development of red-shifted GECIs (e.g. jRCaMP1a,
168 jRCaMP1b, jRGECO1a, jRGECO1b) (Akerboom et al., 2013; Dana et al., 2016; Montagni et al., 2019);
169 these allow the simultaneous use of optogenetic activation of Channelrhodopsins using blue light while
170 recording calcium activity (Akerboom et al., 2013).

172

173 **b. Voltage indicators**

174 Voltage imaging can directly display membrane potential dynamics and has been used to measure
175 neural dynamics for decades (Bando et al., 2019). Genetically-encoded voltage indicators (GEVIs) can
176 be categorised into 3 classes based on their molecular structure and voltage-sensing mechanism:
177 voltage-sensitive domain-based sensors, rhodopsin-based sensors, and rhodopsin-FRET sensors (see
178 (Bando et al., 2019) for a comparative review on GEVIs). While imaging voltage using fluorescent-
179 based sensors appears to be an ideal technique to probe neural circuits with high spatiotemporal
180 resolution, due to insufficient SNR, imaging membrane potential is still challenging, and in order to
181 achieve single action potential resolution *in vivo*, brighter voltage indicators will need to be developed
182 (Aharoni and Hoogland, 2019).

183

184

185 **2. Directing GECIs to neurons of interest**

186 **a. Viral Vectors**

187 Viruses can be used to target Ca²⁺ indicators to specific cells *in vivo*. Adeno-associated virus (AAV)
188 and lentivirus (LV) are the most common viral vectors used today for neuroscience applications and
189 result in robust expression of the desired gene throughout the cell. Due to their low immunogenicity,
190 AAVs and LVs are well tolerated and highly expressed over long periods of time without any reported
191 adverse effects (Kaplitt et al., 1994; Sakuma et al., 2012; Samulski and Muzyczka, 2014) in various

192 species (Vasileva and Jessberger, 2005). AAVs are the most widely used by the scientific community;
193 their efficiency has been evaluated for many brain regions and cell types, and most of them are
194 commercially available from facilities such as Addgene, Penn Vector Core, or ETH Zurich. It is very
195 common to deliver a Cre-dependant viral vector in a Cre-line mutant mouse. With this approach, Ca²⁺
196 indicator cell-type specificity is typically determined by the genetically-controlled presence of a
197 recombinase (Cre) in the specific cells of interest. The viral approach has several advantages, including
198 topographic specificity and the ability to control the amount of protein transduced (adjustment of
199 volume and concentration of viral vectors). However, viral neuronal transfection relies on stereotaxic
200 injection and therefore every animal is unique. Viral vectors also have to be carefully selected and
201 require rigorous post-hoc histological validation.

202 AAVs

203 AAVs are small particles (20nm) allowing them to spread very efficiently within tissues and are
204 particularly well-adapted to brain cell transfection. The choice of the appropriate AAV needs be based
205 on multiple factors, from the physical location of the viral injection in the brain, to the serotype/cell-
206 type affinity of the chosen viral vector, as well as the molecular and genetic machinery driving its
207 replication/integration. AAVs present different serotypes meaning that their capsid proteins differ as
208 well as DNA sequences (inverted terminal repeats, ITRs) that result in variations in speed of viral gene
209 expression onset and target cell specificity. Overall, AAV1, 2, 5, 6, 8, and 9 have different affinities for
210 different cells but should all be able to transfect neurons (Aschauer et al., 2013; Hammond et al., 2017)
211 . When in doubt, AAV-DJ (Grimm et al., 2008) or AAV DJ8 (Hashimoto et al., 2017) may be good
212 options to test out transfection of neurons that have not been studied before due to their alleged
213 increased tissue tropism. Several ubiquitous promoters are available to drive transgene expressions with
214 AAVs; although not exhaustive, Table 1 summarizes serotypes and promoters used to successfully
215 transfect various hypothalamic neuronal populations.

216 Lentiviruses

217 LVs are big particles (80-120nm) and can carry inserts as large as 10kb (as opposed to the limited 4.5
218 kb capacity of AAVs), which is particularly pertinent when working with a promoter-specific virus.
219 Although they are less commonly used than AAVs, LVs are more efficient at transfecting cells *in vitro*,
220 have similar capabilities *in vivo* (but do not spread as widely as AAVs) and do not require making a
221 choice of serotype (Cannon et al., 2011).

222

223 **b. Transgenics**

224 In order to work with animals with similar levels of transgene expression within the targeted neuronal
225 phenotype, transgenic lines have been generated. Essentially, two approaches exist.

226 In the first type of transgenic line, GCaMP is expressed under the control of specific promoters.
227 For example, The Thy1-GCaMP3 (Chen et al., 2012), 6s and 6f (Dana et al., 2014) transgenic mouse
228 lines express GCaMP in Thy1-expressing neurons across the entire brain and have been used for *in*
229 *vitro* and *in vivo* Ca²⁺ imaging. Similarly GCaMP2 expression under the Kv3.1 potassium-channel
230 promoter has been used to perform Ca²⁺ imaging of the glomerular layer of the mouse olfactory bulb
231 (Fletcher et al., 2009). Finally, transgenic rat lines have been developed and Thy1-GCaMP6f rats have
232 been used to record cortical activity with a head-mounted microscope (Scott et al., 2018).

233 The second and more common approach is to generate transgenic animals bearing GCaMP
234 expression in specific cell types, by crossing a Cre-driver with a floxed-GCaMP mouse (Hsiang et al.,
235 2017; Zimmerman et al., 2019). Several floxed-GCaMP mice lines are now commercially available
236 from Jackson laboratories and have been characterised by users. Nevertheless, potential concerns have
237 to be kept in mind if working with transgenics and attention will need to be given to potential ectopic
238 expression, drift and loss of specificity of the transgene, or even disrupted Ca²⁺ dynamics within
239 GCaMP-expressing neurons (Steinmetz et al., 2017). After years of working with GECIs or genetically-
240 addressable opsins, many labs including our own have favoured the use of viruses. Overall, viral vectors
241 lead to a greater level of expression of the desire transgene, which is essential *in vivo*, and generating
242 transgenic lines has been an expensive, time-consuming process that has not always resulted in success.

243

244 **c. Histological validation of GCaMP expression**

245 Regardless of the technique used to target GCaMP to specific cells, it is essential to confirm the extent
246 of transgene expression, spread, and location over the experimental timeline using histology
247 methodologies. Typically, animals will be terminally anesthetized and transcardially perfused with a
248 4% paraformaldehyde solution, and brains will be removed, sectioned and processed for histological
249 analysis. Native GCaMP expression should be bright enough to visualize in fixed sections with
250 epifluorescence or confocal microscopy, with fluorescence signal limited to the cell membrane. Filled
251 nuclei and/or misshapen neurons can be a sign of overexpression, which can be overcome by reducing
252 viral vector concentration.

253 In order to identify transfected neurons with immunohistochemistry techniques, GCaMP
254 labelling can be achieved using a GFP antibody; this is especially useful in situations where GCaMP
255 cannot be clearly detected without enhancement. Alternatively, it is possible to perfuse the animal with
256 calcium-containing DPBS (Dulbecco's Phosphate Buffer Saline). Since DPBS contains a saturating

257 concentration of Ca^{2+} (0.9 mM), GCaMP brightness will be maximal, and the experimenter may
258 therefore be able to visualize GCaMP fluorescence without antibodies (Dana et al., 2014).

259

260 **3. Imaging deep brain areas**

261 While cortical activity can be recorded through cranial window, hypothalamic neuroendocrine neurons
262 are located deep in the brain (from half a centimetre deep for mice to up to a centimetre deep for rats)
263 and it is therefore necessary to find tools that allow the experimenter to see ‘deep inside’ the brain.
264 Fortunately, in parallel to the development of Ca^{2+} indicators, instrumentation was optimized to render
265 Ca^{2+} imaging possible in subcortical brain areas.

266

267 **a. GRIN lenses**

268 GRIN lenses resemble simple glass needles, but they are in fact complex lenses with a radially-varying
269 index of refraction; this causes an optical ray to follow a sinusoidal propagation path through the lens.
270 GRIN lenses combine refraction at the end surfaces along with continuous refraction within the lens.
271 Their characteristics allow them to relay optical images from one end to the other, with very low
272 aberrations for objects near the optical axis. For these reasons, GRIN lenses are the perfect tool to
273 perform *in vivo* imaging in deep-brain regions, relaying signals a point above the skull surface where
274 image acquisition can take place (Barretto et al., 2009). GRIN lenses exist in different lengths and
275 diameters. For brain regions such as the dorsal striatum (Zhang et al., 2019), prelimbic cortex (Pinto
276 and Dan, 2015) or hippocampus (Ziv et al., 2013), a 1 mm diameter GRIN lens can be used to increase
277 the field of view. For deep-brain areas such as the amygdala (Li et al., 2017) or hypothalamus (Jennings
278 et al., 2015), a lens of approximately 0.5mm diameter can be used in order to minimize tissue damage
279 during lens implantation. For neuroendocrine hypothalamic areas (e.g. arcuate nucleus, paraventricular
280 nucleus, rostral preoptic area), we have successfully used 0.6mm diameter 7.4mm long lenses for mice,
281 and 0.8mm diameter 10.8mm long lenses for rats.

282

283 **b. Prism probes**

284 Side-view GRIN lenses or ‘prism-probes’ exist. These are composed of a prism fixed to the bottom of
285 a cylindrical GRIN relay lens. The slanted surface of the prism is coated with metal (aluminium or
286 silver for high reflectivity) to reflect by 90° the light from the microscope to excite GCaMP cells located
287 along the imaging face of the prism probe. The emitted light from the cells also reflects off the
288 hypotenuse of the prism and can be collected through the objective of the microscope. These probes

289 have been used for multi-layer cortical imaging (Gulati et al., 2017) and could be suitable for
290 populations of hypothalamic neurons that are spatially distributed along the z-axis.

291

292

293 **c. GRIN lens implantation**

294 Unravelling the intricacies of neuroendocrine function with *in vivo* imaging studies lasting days to
295 weeks requires optical access to the structure of interest while maintaining both its integrity and that of
296 the surrounding tissue. First of all, before performing GRIN lens implantation in animals, it is sensible
297 to use a ‘phantom brain’ preparation where the GRIN lens is implanted into an agar/fluorescent
298 microbead preparation (Kim et al., 2017). This preparation can be looked at under any epifluorescence
299 microscope in order to verify the working distance of the GRIN lens. GRIN lenses have to be placed
300 above the targeted structure and the space needed between the lens and the neurons is determined by
301 the working distance (50-350µm) of the imaging side of the GRIN.

302 In order to gain optical access to the hypothalamus, a GRIN lens has to be guided through the
303 cortex towards the ventral side of the brain. To overcome the challenge of crossing the meninges and
304 going through the brain tissue without increasing pressure and causing excessive damage, the GRIN
305 lens can be inserted into the lumen of a needle, which can then be retracted once the GRIN lens is
306 located correctly. Practically, the GRIN lens is placed inside a small gauge needle, with movement
307 along the needle restricted by placing a metal rod above it. The needle is then lowered to a point just
308 above the target, and then removed with the metal rod kept in place, ensuring the GRIN lens stays in
309 place. Finally, the metal rod is removed and the GRIN lens fixed in position with dental cement (Hoa
310 et al., 2019). An alternative is to first create a path to the target structure with a needle or a dissection
311 knife (Gulati et al., 2017), and to then lower the naked GRIN lens along this path; in this method, the
312 lens can be carefully held using a bulldog clamp or a pipette tip trimmed to match the diameter of the
313 lens. Another interesting method consists of placing the top part of the GRIN lens inside a glass tube
314 and fixing it using Super Glue. The glass tube can then be held with an electrode holder on the
315 stereotaxic arm. Once the GRIN lens has been positioned in the brain and cemented in place, acetone
316 can be carefully introduced into the glass tube in order to dissolve the Super Glue, thus freeing the
317 GRIN lens (Zhang et al., 2019).

318 GRIN lens implantations are invasive procedures that cause inflammatory responses in the brain, during
319 which the neurons do not behave normally. It is recommended to wait at least 3 weeks after implantation
320 before starting imaging sessions; overall, we have had the most success imaging Ca²⁺ activity from 5
321 weeks to several months after GRIN lens implantation. It is also necessary to ensure that GRIN lens
322 implantations do not result in long-term inflammatory responses that could alter physiological function.

323 Attention therefore needs to be given to possible behavioural/hormonal changes, and post hoc
324 histological validation is necessary.

325 **d. Sourcing GRIN lens**

326 Currently, to our knowledge, there are two manufacturers of GRIN lenses suited to brain imaging
327 applications. The first is GRINTECH, who hold a strategic partnership with the neurotechnology
328 company Inscopix. All GRINTECH lenses used in the field of non-confocal, single photon epi-
329 fluorescence imaging for non-human neuroscience application must be purchased through Inscopix.
330 The second manufacturer is GoFoton, who are the largest manufacturer of GRIN lenses in the world.
331 Although their GRIN lens production has been focused on telecommunication applications and fibre
332 coupling, they have been working over the past year at developing GRIN lenses specifically for brain
333 imaging applications. Hopefully, GoFoton will be able to provide high quality GRIN lenses for
334 microscopic applications in the near future.

335

336 **4. Imaging in conscious animals**

337 Deep-brain imaging of Ca^{2+} activity can be performed through GRIN lenses that are chronically
338 implanted; these relay fluorescence captured inside the brain to the surface of the skull, which can be
339 observed with conventional microscopy techniques. Depending on the research question and the image
340 quality needed, deep-brain imaging can be performed with a bench top microscope on head-restrained
341 animals or with the help of a head-mounted miniature microscope for freely-moving animals.

342

343 **a. Head-fixed configuration**

344 In order to perform deep-brain imaging in conscious animals, rodents can be temporarily restrained
345 under a microscope with the help of a metal piece chronically fixed to their skull. Animals retain the
346 ability to move on a wheel or a cylinder in order to give an impression of movement and reduce stress
347 during the experiments. This approach has been used to perform calcium imaging in deep-brain areas
348 (Bocarsly et al., 2015), and even in two areas at the same time (Lecoq et al., 2014). While most of these
349 studies have been performed using two-photon microscopes, we have successfully performed 1-photon
350 calcium imaging in the hypothalamus of head-fixed mice with a stereomicroscope fitted with a 20x
351 objective (for detailed methodology see (Hoa et al., 2019)). Using this set-up, we investigated the
352 endogenous activity of hypophysiotropic TRH neurons across several days. To do so, we worked with
353 TRH-Cre mice (Krashes et al., 2014) (kindly gifted by Pr. B. Lowell, Beth Israel Deaconess Medical
354 Center & Harvard Medical School) that had been injected with a Cre-dependant AAV driving GCamp6s
355 expression. We recorded the activity of several TRH neurons at single-cell resolution level in head-

356 fixed mice (Fig2). This experimental design enabled us to study how hypophysiotropic TRH neurons
357 interact with each other within local networks and modulate their activity throughout the day (Campos
358 and Mollard, unpublished observations). A great benefit of deep-brain imaging in head-fixed
359 configuration is that bench top microscopes offer excellent imaging quality and it is therefore possible
360 to record the activity of sub-cellular structures (Meng et al., 2019) . Indeed, we have successfully
361 imaged the calcium activity of assemblies of TRH neuron terminals in the median eminence, although
362 1-photon microscopy could not spatially resolve individual boutons (Campos and Mollard, unpublished
363 observations).

364

365 **b. Miniscopes**

366 In 2011, Mark Schnitzer's group first reported the miniature microscope (miniscope) with
367 epifluorescent light source (Ghosh et al., 2011), which was small, light, and easy to mount on the head
368 of a mouse for studying complex behaviours in freely-moving animals. Combined with a GRIN lens,
369 the miniscope imaging system enables recording of calcium activity from hundreds of neurons in deep-
370 brain regions for months, with imaging quality comparable to benchtop microscopes. Over the last 5-
371 10 years, several miniscope designs have emerged, but currently, two miniscopes in particular appear
372 to be widely used: the Inscopix nVista miniscope and the UCLA miniscope. These two miniature
373 microscopes share the same core features. The optical design includes an achromatic lens which focuses
374 near-collimated light from an objective GRIN lens onto a CMOS sensor and a set of optical filters. The
375 plastic housing can be machined or 3D printed, and custom electronics are used to control and read-out
376 the excitation LED light source and CMOS imaging sensor. Miniscopes are connected to a data
377 acquisition (DAQ) box that relays data to a computer. A base plate is attached to the skull of the animal
378 with dental cement and allows magnetic latching of the miniscope to the baseplate.

379 nVista Inscopix Miniscope.

380 The Inscopix company was founded in 2011 by Kunal Ghosh, Mark Schnitzer and Abbas El Gamal in
381 order to commercialise their miniature microscope. Some years later, their technology has evolved and
382 the Inscopix miniature microscope, called nVista, is now widely used. The characteristics of the current
383 version of the nVista microscope are presented in Table 2. It possesses a software-controlled electronic
384 focusing mechanism (300 μm) that does not require any manual intervention. The miniscope is
385 connected to a DAQ box which has the capacity to store data on an SSD and/or an SD card. The DAQ
386 box is also equipped with ethernet and WIFI connectivity, which allows remote control of the miniscope
387 and data streaming through web-based acquisition software.

388 On purchasing the nVista system, researchers will receive a full support package, which makes
389 it probably the easiest way to start working with deep-brain imaging with a miniscope. Researchers will

390 benefit from field scientific consultants that will, through site visits and online communication, help
391 them set up the technology and troubleshoot experimental and conceptual challenges (from Ca²⁺
392 indicator selection, to data analysis) in order to ensure the success of research project. It is worth
393 highlighting that the nVista miniscope comes with a 1-year manufacturer's warranty that can be
394 prolonged to 5 years. For damaged scopes sent back to the company, turn-around time is typically
395 around 1 week. In our own experience, this warranty has been valuable; we have had to return damaged
396 nVista miniscopes to Inscopix 3-4 times per year for repair. This support package comes at a price of
397 course; currently, the nVista system (consisting of one nVista 3.0 scope + accessories + 1-year warranty
398 + help + software) costs in the region of 70-80000 USD.

399

400 UCLA Miniscope

401 The UCLA miniscope is also based on the design pioneered by Mark Schnitzer's Lab, but this miniscope
402 is open-source. The characteristics of the UCLA miniscope version 3 (V3) are presented in Table 2. It
403 also uses a single, flexible coaxial cable to carry power, communication, and data transmission to a
404 custom open source DAQ box and software. The default version of the UCLA miniscope only allows
405 cortical imaging. For imaging deeper brain areas, an objective GRIN lens can be mounted inside the
406 miniscope and positioned above a GRIN relay lens chronically implanted above the target cells.
407 Focusing adjustment (300µm) occurs through a linear slider that can be manually adjusted in height;
408 although it preserves the orientation of neurons between imaging sessions, it can be tricky to use,
409 especially when the miniscope is head-mounted.

410 The UCLA Miniscope has had a significant impact on the neuroscience community, with at
411 least 400 labs around the world building and using these imaging devices for their research studies over
412 the past 3 years. This success is likely due to a broad dissemination policy. The 'miniscope project'
413 began as a collaboration between the Golshani Lab, Silva Lab, and Khakh Lab at the University of
414 California, Los Angeles, and provides documentation, tutorials on part procurement, assembly and
415 experimental application guides, both online and through workshops. The <http://miniscope.org> website
416 provides a centralized hub for users to share design files, source code, and other relevant information
417 related to this imaging technique.

418 Building a UCLA miniscope is cost-effective (DAQ + 1 scope < \$1,000 USD). It is not
419 complicated but does require soldering and hands-on assembly. A main advantage is that it can be tuned
420 to fit the research project requirements, and additionally by building it, researchers understand how to
421 fix it quickly. For those that do not feel confident building the miniscope, LabMaker
422 (www.labmaker.org), based in Berlin, Germany, sell the UCLA miniscope as a kit that does not require
423 any soldering for approximately \$2,000 USD (includes DAQ + 1 scope).

424

425 Improvements of the UCLA miniscope

426 It is worth noting that this is a rapidly-evolving field, with technological improvements in miniature
427 microscopes emerging all the time. For example, at the time of writing, a new version (V4) of the UCLA
428 miniscope has just been released (<http://miniscope.org>). Compared to the UCLA V3 miniscope, the V4
429 miniscope is lighter (2.6g), utilises a smaller baseplate (25 µm footprint), has a field of view that can
430 be set based on the combination of lenses used when assembling the miniscope (1000 µm-diameter or
431 more), has an improved CMOS that requires just a fifth of the excitation power of previous systems, and
432 is expected to have improved resolution (0.5MP) and faster imaging speed (120FPS) (Daniel Aharoni,
433 2019 Neuro Open-source Workshop, January 2019). In addition, the manual focusing mechanism of
434 V3 has been replaced by an electronic system. Indeed, similar to the nVista system, the V4 miniscope
435 benefits from liquid lenses that consist of an interface of two immiscible liquids which, under voltage,
436 deform and act as a lens allowing for electronic focusing without the need for manual adjustment. This
437 should make focusing much easier, and because liquid lenses can be adjusted rapidly, it may become
438 possible to perform interleaved recording from different focal planes (Aharoni and Hoogland, 2019).
439 Finally, in order to allow for simultaneous two-colour fluorescence imaging, the objective GRIN lenses
440 present in the previous version of the UCLA miniscopes that created chromatic aberrations, have been
441 replaced in V4 miniscopes by achromatic lenses (Aharoni and Hoogland, 2019). However, since deep-
442 brain imaging necessitates the implantation of GRIN lenses in the brain, this new feature does not yet
443 represent an advantage for the study of deeply-located neuroendocrine cells. It is important to note that
444 although the UCLA V4 miniscope possesses promising improvements and can be fitted with relay
445 GRIN lenses for deep brain imaging, to our knowledge, they have not yet been tested for structures
446 deeper than the cortex. The V4 is expected to be released as a kit in 2020.

447

448 **c. Alternatives and next generation miniscopes**

449 Wire-free scopes

450 Whilst tethered systems are currently the most effective method for *in vivo* recording/control of freely-
451 moving animals, wireless (Liberti et al., 2017) and wire-free (Shuman et al., 2018) open-source
452 miniscopes have been developed with the latest being used to record CA1 place cells during maze
453 navigation in epileptic mice. These recent studies have demonstrated the feasibility of using a
454 lightweight wireless miniature microscope system to transmit Ca²⁺ imaging data to a receiver (Liberti
455 et al., 2017) or save data directly to a microSD card positioned on the miniscope (Shuman et al., 2018).
456 Both designs are powered by onboard lithium polymer batteries that can be attached to the microscope
457 body or mounted on the back of the animal, consequently adding weight to the microscope design (~2

458 g for a 50 mAh battery). Alternatively, wireless powering of a miniaturized design with low power
459 consumption is thought to be feasible with near-field wireless power transfer similar to those that have
460 already been implemented for wireless optogenetic stimulation (Aharoni and Hoogland, 2019). While
461 power consumption (which scales with data bandwidth) is one of the limiting factors in designing a
462 miniaturized wireless microscope due to battery size and weight requirements, power-efficient CMOS
463 imaging sensors can be used along with pixel binning or pixel subsampling to minimize power
464 consumption while maintaining a comparable field of view, albeit at a lower resolution than is possible
465 using tethered systems (Aharoni and Hoogland, 2019). The open-source nature of ongoing miniscope
466 projects allows for the rapid sharing of designs, modifications and ideas across laboratories, and it is
467 expected that wireless systems will rapidly improve and that their use will soon escalate within the
468 neuroscience community. Of particular interest here is Open-ePhys, a non-profit initiative
469 encompassing a large team of scientists and developers, which has released a kit to convert the wired
470 UCLA miniscope (version 3) into a wire-free system.

471

472 Two-Photon imaging

473 Two-photon (2P) excitation improves optical sectioning of samples and thereby ensures that the light
474 collected is only from the cellular and subcellular structures that lie along the focal plane of 2P
475 excitation. While 2P brain imaging in animal models usually requires that the animal is head-fixed,
476 there have been several successful attempts at building a 2P miniscope (see (Helmchen et al., 2013) for
477 review) with some designs used to image in freely-moving rodents (Ozbay et al., 2018; Zong et al.,
478 2017). A major disadvantage to this technique is that it requires expensive table-top lasers coupled to
479 optical fibres to achieve 2P excitation (Aharoni and Hoogland, 2019). Furthermore, a recent study
480 compared data acquired with a 2P benchtop microscope with one-photon images acquired with a
481 miniscope, and found that orientation tuning of the same identified neurons was comparable
482 irrespective of the type of fluorescence excitation used (Glas et al., 2019).

483

484

485 **5. Animal handling**

486 Regardless of the imaging technique, it is important to take the time to handle animals to ensure they
487 become familiar with the experimenter and being moved in and out of their cage. It is possible to quickly
488 and briefly anaesthetise the animal when attaching the miniscope or placing the animal in the head-
489 attached set-up, but it is not recommended. Indeed, as discussed later in this review, anaesthetics, even
490 when used for a very short period of time, may affect neuronal dynamics, lead to changes in hormone
491 secretion, or alter animal behaviour.

492

493 **a. Head-fixed habituation**

494 For head-fixed experiments, it is useful to place the animal under the microscope for a few minutes
495 every day leading up to the experiment. Attention should be paid to details such as lighting, electrical
496 equipment, and ventilation in order for the animal to acclimatise to the exact conditions that will be
497 used for the experiment. It is also important to protect the animal's eyes from the microscope's
498 excitation light by covering the front part of the head with suitable opaque material. We have found that
499 animals never get completely used to being head restrained for long periods of time, but studies have
500 reported self-initiated head-fixation system for functional imaging in mice. For example, mice have
501 been shown to self-initiate head-fixation in order to get water, enabling imaging to be performed
502 through cranial windows (Aoki et al., 2017; Murphy et al., 2016). Although it has never been used for
503 deep-brain imaging, this habituation technique seems promising and shows that with patience and good
504 experimental design it is indeed feasible to perform imaging in 'low stress' head-fixed animals.

505

506 **b. Miniscope habituation**

507 For miniscope experiments, the acclimatisation process is more straightforward. Animals should first
508 habituate to their imaging arena for a few minutes each day leading up to the experiment. Then, it is
509 important for the animals to get used to carrying the miniscope, which can weigh about 10% of the
510 weight of an adult mouse. We use 'dummy' miniscopes to train our animals; they are of the exact same
511 weight and size as the real miniscope and are connected using the same type of cable. We have found
512 that animals carrying dummies for a few days soon behave in a completely normal way. It is also useful
513 to use a dummy miniscope so the animals get used to the microscope cable. Indeed, mice will try to
514 chew on the cable, and we have found that coating the dummy cable with bitter nail polish usually
515 prevents mice from chewing the real cable during experiments. We have yet to try this methodology
516 with rats.

517

518 **c. Evaluating stress**

519 Together with handling and habituation, it is recommended to evaluate the level of stress of the animals
520 throughout the experiments by measuring corticosterone concentration. Commercially-available
521 enzyme-linked immunosorbent assay (ELISA) kits are widely used to quantify corticosterone levels for
522 the assessment of stress in laboratory animals. Some of them, such as the AssayMax corticosterone
523 ELISA kit (AssayPro), only require small volumes of whole blood (3-6 μ L per sample) that can be
524 collected using a minimally-invasive technique such as tail-tip blood sampling (Guillou et al., 2015).
525 Although the precision in determining true values of corticosterone is low for commercial ELISA kits,

526 they have proven to be useful to determine relative differences within studies (e.g. head-fixed animals
527 vs. freely-moving animals vs. sham animals).

528

529

530 **6. Analysis**

531 *In vivo* Ca²⁺ imaging using GRIN lenses and 1-photon-based microscopes enables the study of neural
532 activities in behaving animals which would be impossible using other techniques. However, the high
533 and fluctuating background fluorescence, inevitable movement and distortion of the imaging field, and
534 extensive spatial overlaps of fluorescent signals emitted from imaged neurons, present major challenges
535 for extracting neuronal signals from the raw imaging data (Lu et al., 2018). Overall, the experimenter
536 will need to identify the spatial outline of each neuron in the field of view, untwine spatially-overlapping
537 neurons, and finally deconvolve the spiking activity of each neuron from the dynamics of the Ca²⁺
538 indicator.

539

540 **a. Enhancement and Motion correction**

541 Overall, several steps are necessary to obtain valuable signals. First, the data needs to be ‘enhanced’ by
542 applying a spatial filter that enhances the signal intensity and removes as much background noise as
543 possible. It is then necessary to perform movement correction in order to align (or register) images.
544 This step not only helps correct for movement that can occur when animals are grooming, chewing
545 etc..., but also helps with brain tissue movement in areas close to ventricles. Indeed, we have observed
546 that the brain shows movement even when animals are static, which we hypothesise is due, at least in
547 part, to cerebral spinal fluid flowing through the ventricles. Non-rigid motion-correction algorithms that
548 run on Fiji (such as Moco (Dubbs et al., 2016)) or Matlab (such as NoRMCorre (Pnevmatikakis and
549 Giovannucci, 2017)) have proven useful in solving large-scale image registration problems.

550

551 **b. Extraction of calcium signals in regions of interest**

552 When images have been treated and motion corrected, they are ready to be analysed. Fluorescence in
553 regions of interest (ROI) can be measured over time. The selection of ROI can easily be done by hand
554 (ROI Manager in Fiji) in very scattered populations, but for large data sets that contain a dense
555 populations of neurons, automated cell-sorting algorithms may be better suited to extract spatial and
556 temporal properties of individual cellular Ca²⁺ signals (Mukamel et al., 2009; Pnevmatikakis et al.,
557 2016). In brief, most cell identification algorithms run principal component analysis (PCA) to

558 remove signals that mostly encode noise. Dimension reduction is then followed by independent
559 component analysis (ICA) to identify the spatial and temporal properties of visualized cells by
560 segmenting the data into statistically-independent spatial and temporal signals. PCA/ICA relies on
561 statistical independence of signals and fluorescent signals will be identified as cells only if their
562 activities are not synchronised and if they do not have the same pixel coordinates. The extracted signals
563 can then be manually sorted to confirm that they represent cellular Ca^{2+} transients from spatially-defined
564 GCaMP-expressing cells. This technique is particularly helpful for the analysis of dense populations
565 and allows the rapid identification of thousands of neurons (Jennings et al., 2015; Ziv et al., 2013), but
566 has also been used to successfully extract individual cellular signals from relatively sparse neuronal
567 populations such as AGRP neurons located within the arcuate nucleus (Betley et al., 2015).
568 Alternatively, constrained nonnegative matrix factorization (CNMF) approaches have been developed
569 for *in vivo* Ca^{2+} recording analysis (Zhou et al., 2018) that have proven to be more accurate than
570 PCA/ICA methods. The main advantage is that CNMF methods have the capability of demixing
571 spatially-overlapping neurons. The CNMF-E (Constrained Nonnegative Matrix Factorization for
572 microEndoscopic data) variant has an added model to estimate and account for time-varying
573 background fluctuations in fluorescence (Aharoni and Hoogland, 2019; Zhou et al., 2018). It is however
574 important to note that all computational methods also have limitations that can reduce the accuracy of
575 data interpretation (Resendez et al., 2016), and it is currently unclear which method is best suited for
576 Ca^{2+} indicator data from epifluorescence deep-brain imaging. For a complete review of Ca^{2+} imaging
577 data analysis and alternative techniques see (Pnevmatikakis, 2019).

578

579 **c. Spike detection**

580 Spike inference methods aim to estimate the spike times of a neuron given its isolated fluorescence
581 trace. After ROIs of each active neuron have been identified, $\delta F/F$ traces can be extracted then
582 deconvolved to approximate spiking activity of each segment. This process can be challenging due to
583 the unknown and often non-linear nature of the indicator dynamics, the presence of measurement noise,
584 and the relatively low imaging rate of typical recordings (Pnevmatikakis, 2019). While CNMF methods
585 have been successfully used to infer spikes, it should be emphasized that the signal reported by a
586 fluorescent indicator is a convolution of the Ca^{2+} transients and the indicator response. Although a good
587 temporal relationship between neuronal firing and GCaMP signals has been reported for several
588 neuronal cell types (Chen et al., 2013; Dana et al., 2018), this relationship cannot be taken for granted
589 and Ca^{2+} transients should not be seen as electrical recordings. In order to help with the interpretation
590 of *in vivo* GCaMP fluorescence dynamics in specific neuronal populations, it can be informative to
591 undertake dual electrical- Ca^{2+} imaging experiments in targeted neurons *in vitro* before performing *in*
592 *vivo* experiments.

593

594 **d. Analysis packages**

595 To facilitate the management of big data sets as well as data analysis by non-experts, open access
596 analysis packages have become available and are constantly improving. The following three packages
597 have been used successfully by the miniscope community: (1) CaImAn, a computational toolbox for
598 large scale calcium imaging analysis, which includes movie handling, motion correction, source
599 extraction, spike deconvolution and result visualisation (Giovannucci et al., 2019), which is the most
600 up-to-date package; (2) MiniscoPy, a python-based package adapted from CaImAn specifically to
601 analyse miniscope recordings (Zhou et al., 2018); and (3) MiniscopeAnalysis, an updated version of
602 the initial miniscope analysis package developed for the miniscope project. As an alternative to these
603 packages, Lu and colleagues (Lu et al., 2018) have developed a fully-automated algorithm called the
604 miniscope 1-photon imaging pipeline (MIN1PIPE), which contains several stand-alone modules and
605 can handle a wide range of imaging conditions and qualities with minimal parameter tuning, and
606 automatically and accurately isolate spatially-localized neural signals. We have worked with
607 MIN1PIPE and found it efficient and easy to use and adapt to our needs without having to be a specialist
608 in data analysis.

609 Inscopix clients will benefit from the user-friendly ‘Inscopix Data Processing’ software that
610 performs all steps of the analysis (filter, motion correction, cell registration for longitudinal studies,
611 extraction of the signal) with very limited parameter tuning. We have found it very easy to use and
612 convenient for recordings with good SNR and limited motion artefacts.

613

614 **e. Computer/hard disk specifications**

615 The high-definition data acquired during Ca^{2+} imaging sessions require a significant amount of hard
616 disk space during recording (acquiring 30 minutes of data at the frame rate of 20 Hz with the nVista
617 miniscope requires approximately 110 GB of hard disk space) as well as a substantial amount of space
618 for data storage. This problem should be thought through before starting any recordings. Moreover, in
619 order to perform longitudinal studies, movies from different recording sessions will need to be
620 concatenated into a single large file, and powerful computers with numerous cores will be required for
621 analysis.

622

623

624 **7. Readout and physiological consequence of the signals recorded**

625 Once the recordings have been analysed and spatial and temporal data have been extracted, it can still
626 be a challenge to understand the signals. Indeed, within a defined neuronal population, subgroups or
627 individual neurons may be active at different time points, so it is critical to find ways to distinguish the
628 activity we are interested in from the rest.

629

630 **a. Behavioural/Environmental changes**

631 One of the most notable benefits provided by *in vivo* imaging of neuronal activity in conscious animals
632 is that it is possible to correlate the signal with contextual changes in environment (e.g. time of the day,
633 temperature, light intensity), behaviour (e.g. environmental exploration, time-locked stimulus
634 presentations), or pharmacological induced alterations of network activity. Indeed, the ability to image
635 cell type-specific activity during naturalistic animal behaviour allows this imaging protocol to be
636 applied to a wide array of experimental manipulations, not only to answer questions that could not be
637 tackled using previous methods for monitoring of neural activity, but to provide clues about the
638 significance of the recorded calcium signals. With the ability to record activity across several
639 days/weeks, each animal can become its own control. But what is perhaps more valuable is that because
640 individual neurons can be registered and therefore studied over several recording sessions, each neuron
641 can become its own control. We have used this experimental design to study the effect of isoflurane on
642 hypothalamic neuronal activity. General anaesthetics, especially isoflurane, are routinely used to induce
643 a sleep-like state, allowing otherwise painful or stressful procedures to be performed, but have been
644 long known to alter hormonal secretion. For example, in rats fed ad libidum, isoflurane increases
645 glycemia, glucagon and GH levels but causes decreases in insulin, ACTH and corticosterone levels
646 (Saha et al., 2005). Similarly, pulsatile LH secretion and LH concentrations are diminished in
647 anaesthetised mouse models (Campos and Herbison, 2014). How exactly isoflurane works in the brain
648 is not fully understood (Campagna et al., 2003), and although its effect on neurons has not been studied
649 in real time *in vivo*, studies have reported disrupted calcium activity in astrocytes (Thrane et al., 2012)
650 and altered blood flow in the brain (Rungta et al., 2017) following isoflurane anaesthesia. Armed with
651 the ability to image hypothalamic neurons *in situ*, we have been able to characterise the effect of
652 isoflurane on the Ca²⁺ dynamics of arcuate nucleus neurons. We performed Ca²⁺ imaging in head-
653 restrained mice first in awake conditions, and then for a 25-minute period following anaesthesia
654 induction. We monitored the same neurons in both conditions and found that isoflurane greatly altered
655 the Ca²⁺ activity of the recorded neurons-(Fig3) (Campos and Mollard, unpublished observations).

656

657 **b. Blood sampling**

658 An important advantage of working with neuroendocrine circuits is that the final readout of the network
659 and its physiological relevance can in many cases be readily assessed through changes in circulating
660 hormone concentrations. The recent advance in ultra-sensitive hormone assays for pituitary hormones
661 (Guillou et al., 2015; Steyn et al., 2011, 2013) have allowed researchers to increase the sampling
662 frequency while decreasing blood volumes needed to get a high-resolution reading of hormonal
663 dynamics. Two main techniques can be effectively combined with *in vivo* imaging of hypothalamic
664 neurons.

665 Tail-tip method

666 The tail-tip technique involves cutting the last 1mm of tail tip and then collecting small 3 to 5µL
667 volumes of blood that can be analysed for hormone concentration using ultra-sensitive assays. The
668 blood flow is encouraged by gently massaging the tail and stops spontaneously when stroking is
669 stopped. Because of the size of the samples this technique results in minimal blood loss and has been
670 shown to be very efficient in characterising LH and GH profiles in mice (Steyn et al., 2011, 2013). To
671 succeed in using this blood sampling method thorough training is necessary, particularly as animals will
672 be either tethered or head-restrained. Animals need to get used to staying in the hand of the
673 experimenter, being restrained by holding the base of the tail, and having their tail massaged. It is
674 important to note that rats are more sensitive than mice with their tail, and we have failed to measure
675 LH surges in female rats after taking frequent blood samples using this technique.

676

677 Automated blood sampling

678 To collect a series of blood samples at high frequency, animals can be implanted with vascular
679 cannula(s) and connected to an automated blood sampling (ABS) system. These systems withdraw
680 small blood samples via the vascular cannula, which are sent to a fraction collector where they are
681 deposited into collection tubes. The advantage of ABS systems is that the blood sampling procedure
682 can be carried out with minimal disturbance to the animal, and the sampling frequency can be specified
683 according to the goal of the study. These experiments are considered stress-free for the animals and
684 have been used extensively to study the regulation of the hypothalamic-pituitary-adrenal axis (Walker
685 et al., 2012; Windle et al., 1998). There are, however, some disadvantages to this technique. First, the
686 animals need to be implanted with a vascular cannula placed in the jugular vein. Because of the
687 difficulty of this surgery, these experiments, although possible in mice (Adams et al., 2015) are better-
688 suited to larger rodents such as rats. Second, the sample volumes are typically greater than those
689 collected using the tail-tip technique. Third, this technique is particularly suited for the measurement of

690 stable hormones such as corticosterone (Walker et al., 2012). Finally, as animals need to be tethered to
691 perform ABS studies, attention is required to ensure the cable from the miniscope does not become
692 tangled.

693

694

695 • **Conclusions**

696 Deep-brain imaging techniques have the potential to produce data that were long thought impossible to
697 obtain because of the inaccessibility of the hypothalamic-pituitary system. Overall, being able to study
698 the activity of specific hypothalamic neurons in awake animals and in real time offers an incredible and
699 invaluable opportunity to broaden our understanding of how the brain controls endocrine function. It
700 also gives us the opportunity to study why endocrine functions become disrupted in pathophysiological
701 conditions, and how these changes may lead to the development or even protection from pathological
702 consequences. Furthermore, *in vivo* brain imaging in conscious animals permits longitudinal studies,
703 thus offering the capability to use animals (and even individual neurons) as internal controls prior to a
704 challenge (e.g. stress, pregnancy, circadian perturbation), which is in-line with 3Rs guidelines and
705 compares favourably with approaches involving numerous animals to provide adequate n numbers in
706 test and control groups. While these techniques were long thought to be available only to laboratories
707 specialised in optics and engineering, or to laboratories with sufficient funding to purchase ready-made
708 equipment, they are now assessible to the wider endocrine field with the help of open source resources.
709 It is expected that high-quality research and high-impact publications emerging from these
710 methodologies will benefit the scientific and medical communities and open up new research
711 opportunities. While this review has focused on imaging Ca^{2+} dynamics within neurons, many other
712 indicators exist. Of particular interest are Flamingo (Odaka et al., 2014) and R-FlincaA (Ohta et al.,
713 2018), which are single-wavelength indicators that permit imaging of 3'5'-cyclic adenosine
714 monophosphate (cAMP) dynamics in living organisms. Likewise iATPSnFRS allows imaging of
715 extracellular and cytosolic adenosine triphosphate (ATP) in astrocytes and neurons (Lobas et al., 2019).
716 Intensive efforts have also resulted in the development of modified G-protein-coupled receptors in
717 which a permuted GFP has been inserted into the third loop in order to monitor various signalling
718 molecules. While this technology currently only works for the detection of small neurotransmitters such
719 as acetylcholine (Jing et al., 2018) and dopamine (Patriarchi et al., 2018), one can hope that these tools
720 will soon be suitable for *in vivo* detection of peptides and neuropeptides.

721

722

723

724

725 **Acknowledgments :** The authors acknowledge Pr.Bradley Lowell for kindly providing TRH-Cre mice.
726 PC and JJW acknowledge financial support from the Medical Research Council (fellowship
727 MR/N008936/1 to JJW) and the Engineering and Physical Sciences Research Council (grant
728 EP/N014391/1 to JJW). PC and PM acknowledge financial support from the Agence Nationale de la
729 Recherche (ANR-15-CE14-0012-01, ANR-18-CE14-0017-01), France-Bioimaging (INBS10-
730 GaL/AR-11/12), Institut National de la Santé et de la Recherche Médicale, Centre National de la
731 Recherche Scientifique, Université de Montpellier, and Fondation pour la Recherche Médicale
732 (DEQ20150331732).

733

734

735

736

737 **Declaration of interest:** The authors declare that there is no conflict of interest that could be
738 perceived as prejudicing the impartiality of the research reported.

739

740

741

742

743

744

745

746

747

748

749

750

751

752

753

754

755

756

757 • **References**

758 Adams, J.M., Otero-Corchon, V., Hammond, G.L., Veldhuis, J.D., Qi, N., Low, M.J., 2015.

759 Somatostatin is essential for the sexual dimorphism of GH secretion, corticosteroid-binding
760 globulin production, and corticosterone levels in mice. *Endocrinology* 156, 1052–1065.

761 Aharoni, D., Hoogland, T.M., 2019. Circuit Investigations With Open-Source Miniaturized

762 Microscopes: Past, Present and Future. *Front. Cell. Neurosci.* 13, 141.

763 Akerboom, J., Carreras Calderón, N., Tian, L., Wabnig, S., Prigge, M., Tolö, J., Gordus, A., Orger,

764 M.B., Severi, K.E., Macklin, J.J., et al., 2013. Genetically encoded calcium indicators for

765 multi-color neural activity imaging and combination with optogenetics. *Front. Mol. Neurosci.*

766 6, 2.

767 Aoki, R., Tsubota, T., Goya, Y., Benucci, A., 2017. An automated platform for high-throughput

768 mouse behavior and physiology with voluntary head-fixation. *Nat. Commun.* 8, 1196.

769 Aschauer, D.F., Kreuz, S., Rumpel, S., 2013. Analysis of transduction efficiency, tropism and axonal

770 transport of AAV serotypes 1, 2, 5, 6, 8 and 9 in the mouse brain. *PLoS One* 8, e76310.

771 Atasoy, D., Betley, J.N., Su, H.H., Sternson, S.M., 2012. Deconstruction of a neural circuit for

772 hunger. *Nature* 488, 172–177.

773 Bando, Y., Sakamoto, M., Kim, S., Ayzenshtat, I., Yuste, R., 2019. Comparative Evaluation of

774 Genetically Encoded Voltage Indicators. *Cell Rep.* 26, 802-813.e4.

775 Barretto, R.P.J., Messerschmidt, B., Schnitzer, M.J., 2009. In vivo fluorescence imaging with high-

776 resolution microlenses. *Nat. Methods* 6, 511–512.

777 Betley, J.N., Xu, S., Cao, Z.F.H., Gong, R., Magnus, C.J., Yu, Y., Sternson, S.M., 2015. Neurons for

778 hunger and thirst transmit a negative-valence teaching signal. *Nature* 521, 180–185.

779 Bocarsly, M.E., Jiang, W.-C., Wang, C., Dudman, J.T., Ji, N., Aponte, Y., 2015. Minimally invasive

780 microendoscopy system for in vivo functional imaging of deep nuclei in the mouse brain.

781 *Biomed. Opt. Express* 6, 4546–4556.

782 Campagna, J.A., Miller, K.W., Forman, S.A., 2003. Mechanisms of actions of inhaled anesthetics. *N.*

783 *Engl. J. Med.* 348, 2110–2124.

784 Campos, P., Herbison, A.E., 2014. Optogenetic activation of GnRH neurons reveals minimal

785 requirements for pulsatile luteinizing hormone secretion. *Proc. Natl. Acad. Sci. U. S. A.* 111,

786 18387–18392.

787 Cannon, J.R., Sew, T., Montero, L., Burton, E.A., Greenamyre, J.T., 2011. Pseudotype-dependent
788 lentiviral transduction of astrocytes or neurons in the rat substantia nigra. *Exp. Neurol.* 228,
789 41–52.

790 Chen, Q., Cichon, J., Wang, W., Qiu, L., Lee, S.-J.R., Campbell, N.R., Destefino, N., Goard, M.J., Fu,
791 Z., Yasuda, R., et al., 2012. Imaging neural activity using Thy1-GCaMP transgenic mice.
792 *Neuron* 76, 297–308.

793 Chen, T.-W., Wardill, T.J., Sun, Y., Pulver, S.R., Renninger, S.L., Baohan, A., Schreiter, E.R., Kerr,
794 R.A., Orger, M.B., Jayaraman, V., et al., 2013. Ultrasensitive fluorescent proteins for imaging
795 neuronal activity. *Nature* 499, 295–300.

796 Clarkson, J., Han, S.Y., Piet, R., McLennan, T., Kane, G.M., Ng, J., Porteous, R.W., Kim, J.S.,
797 Colledge, W.H., Iremonger, K.J., et al., 2017. Definition of the hypothalamic GnRH pulse
798 generator in mice. *Proc. Natl. Acad. Sci. U. S. A.* 114, E10216–E10223.

799 Cobbold, P.H., Rink, T.J., 1987. Fluorescence and bioluminescence measurement of cytoplasmic free
800 calcium. *Biochem. J.* 248, 313–328.

801 Crick, F., 1999. The impact of molecular biology on neuroscience. *Philos. Trans. R. Soc. Lond. B.*
802 *Biol. Sci.* 354, 2021–2025.

803 Dana, H., Chen, T.-W., Hu, A., Shields, B.C., Guo, C., Looger, L.L., Kim, D.S., Svoboda, K., 2014.
804 Thy1-GCaMP6 transgenic mice for neuronal population imaging in vivo. *PLoS One* 9,
805 e108697.

806 Dana, H., Mohar, B., Sun, Y., Narayan, S., Gordus, A., Hasseman, J.P., Tsegaye, G., Holt, G.T., Hu, A.,
807 Walpita, D., et al., 2016. Sensitive red protein calcium indicators for imaging neural activity.
808 *eLife* 5.

809 Dana, H., Sun, Y., Mohar, B., Hulse, B., Hasseman, J.P., Tsegaye, G., Tsang, A., Wong, A., Patel, R.,
810 Macklin, J.J., et al., 2018. High-performance GFP-based calcium indicators for imaging
811 activity in neuronal populations and microcompartments. *bioRxiv* 434589.

812 Dana, H., Sun, Y., Mohar, B., Hulse, B.K., Kerlin, A.M., Hasseman, J.P., Tsegaye, G., Tsang, A.,
813 Wong, A., Patel, R., et al., 2019. High-performance calcium sensors for imaging activity in
814 neuronal populations and microcompartments. *Nat. Methods* 16, 649–657.

815 Dubbs, A., Guevara, J., Yuste, R., 2016. moco: Fast Motion Correction for Calcium Imaging. *Front.*
816 *Neuroinformatics* 10, 6.

817 Fenno, L., Yizhar, O., Deisseroth, K., 2011. The development and application of optogenetics. *Annu.*
818 *Rev. Neurosci.* 34, 389–412.

819 Fiala, A., Spall, T., Diegelmann, S., Eisermann, B., Sachse, S., Devaud, J.-M., Buchner, E., Galizia,
820 C.G., 2002. Genetically expressed cameleon in *Drosophila melanogaster* is used to visualize
821 olfactory information in projection neurons. *Curr. Biol.* CB 12, 1877–1884.

822 Fletcher, M.L., Masurkar, A.V., Xing, J., Imamura, F., Xiong, W., Nagayama, S., Mutoh, H., Greer,
823 C.A., Knöpfel, T., Chen, W.R., 2009. Optical imaging of postsynaptic odor representation in
824 the glomerular layer of the mouse olfactory bulb. *J. Neurophysiol.* 102, 817–830.

825 Füzesi, T., Daviu, N., Wamstecker Cusulin, J.I., Bonin, R.P., Bains, J.S., 2016. Hypothalamic CRH
826 neurons orchestrate complex behaviours after stress. *Nat. Commun.* 7, 11937.

827 Ghosh, K.K., Burns, L.D., Cocker, E.D., Nimmerjahn, A., Ziv, Y., Gamal, A.E., Schnitzer, M.J.,
828 2011. Miniaturized integration of a fluorescence microscope. *Nat. Methods* 8, 871–878.

829 Giovannucci, A., Friedrich, J., Gunn, P., Kalfon, J., Brown, B.L., Koay, S.A., Taxidis, J., Najafi, F.,
830 Gauthier, J.L., Zhou, et al., 2019. CaImAn an open source tool for scalable calcium imaging
831 data analysis. *eLife* 8.

832 Glas, A., Hübener, M., Bonhoeffer, T., Goltstein, P.M., 2019. Benchmarking miniaturized
833 microscopy against two-photon calcium imaging using single-cell orientation tuning in mouse
834 visual cortex. *PLoS One* 14, e0214954.

835 Grimm, D., Lee, J.S., Wang, L., Desai, T., Akache, B., Storm, T.A., Kay, M.A., 2008. In vitro and in
836 vivo gene therapy vector evolution via multispecies interbreeding and retargeting of adeno-
837 associated viruses. *J. Virol.* 82, 5887–5911.

838 Grynkiewicz, G., Poenie, M., Tsien, R.Y., 1985. A new generation of Ca²⁺ indicators with greatly
839 improved fluorescence properties. *J. Biol. Chem.* 260, 3440–3450.

840 Guillou, A., Romanò, N., Steyn, F., Abitbol, K., Le Tissier, P., Bonnefont, X., Chen, C., Mollard, P.,
841 Martin, A.O., 2015. Assessment of lactotroph axis functionality in mice: longitudinal
842 monitoring of PRL secretion by ultrasensitive-ELISA. *Endocrinology* 156, 1924–1930.

843 Gulati, S., Cao, V.Y., Otte, S., 2017. Multi-layer Cortical Ca²⁺ Imaging in Freely Moving Mice with
844 Prism Probes and Miniaturized Fluorescence Microscopy. *J. Vis. Exp. JoVE*.

845 Hammond, S.L., Leek, A.N., Richman, E.H., Tjalkens, R.B., 2017. Cellular selectivity of AAV
846 serotypes for gene delivery in neurons and astrocytes by neonatal intracerebroventricular
847 injection. *PLoS One* 12, e0188830.

848 Han, S.Y., McLennan, T., Czielesky, K., Herbison, A.E., 2015. Selective optogenetic activation of
849 arcuate kisspeptin neurons generates pulsatile luteinizing hormone secretion. *Proc. Natl.*
850 *Acad. Sci. U. S. A.* 112, 13109–13114.

851 Hashimoto, H., Mizushima, T., Chijiwa, T., Nakamura, M., Suemizu, H., 2017. Efficient production
852 of recombinant adeno-associated viral vector, serotype DJ/8, carrying the GFP gene. *Virus*
853 *Res.* 238, 63–68.

854 Helmchen, F., Denk, W., Kerr, J.N.D., 2013. Miniaturization of two-photon microscopy for imaging
855 in freely moving animals. *Cold Spring Harb. Protoc.* 2013, 904–913.

856 Hoa, O., Lafont, C., Fontanaud, P., Guillou, A., Kemkem, Y., Kineman, R.D., Luque, R.M.,
857 Fiordelisio Coll, T., Le Tissier, P., Mollard, P., 2019. Imaging and Manipulating Pituitary
858 Function in the Awake Mouse. *Endocrinology* 160, 2271–2281.

859 Hsiang, J.-C., Johnson, K.P., Madisen, L., Zeng, H., Kerschensteiner, D., 2017. Local processing in
860 neurites of VGluT3-expressing amacrine cells differentially organizes visual information.
861 *eLife* 6.

862 Jennings, J.H., Ung, R.L., Resendez, S.L., Stamatakis, A.M., Taylor, J.G., Huang, J., Veleta, K.,
863 Kantak, P.A., Aita, M., Shilling-Scrivero, K., et al., 2015. Visualizing hypothalamic network
864 dynamics for appetitive and consummatory behaviors. *Cell* 160, 516–527.

865 Jing, M., Zhang, P., Wang, G., Feng, J., Mesik, L., Zeng, J., Jiang, H., Wang, S., Looby, J.C.,
866 Guagliardo, N.A., et al., 2018. A genetically encoded fluorescent acetylcholine indicator for
867 in vitro and in vivo studies. *Nat. Biotechnol.* 36, 726–737.

868 Kaplitt, M.G., Leone, P., Samulski, R.J., Xiao, X., Pfaff, D.W., O'Malley, K.L., During, M.J., 1994.
869 Long-term gene expression and phenotypic correction using adeno-associated virus vectors in
870 the mammalian brain. *Nat. Genet.* 8, 148–154.

871 Kim, G., Nagarajan, N., Pastuzyn, E., Jenks, K., Capecchi, M., Shepherd, J., Menon, R., 2017. Deep-
872 brain imaging via epi-fluorescence Computational Cannula Microscopy. *Sci. Rep.* 7, 44791.

873 Kim, P., Puoris'haag, M., Côté, D., Lin, C.P., Yun, S.H., 2008. In vivo confocal and multiphoton
874 microendoscopy. *J. Biomed. Opt.* 13, 010501.

875 Kirilov, M., Clarkson, J., Liu, X., Roa, J., Campos, P., Porteous, R., Schütz, G., Herbison, A.E., 2013.
876 Dependence of fertility on kisspeptin-Gpr54 signaling at the GnRH neuron. *Nat. Commun.* 4,
877 2492.

878 Krashes, M.J., Shah, B.P., Madara, J.C., Olson, D.P., Strohlic, D.E., Garfield, A.S., Vong, L., Pei,
879 H., Watabe-Uchida, M., Uchida, N., et al., 2014. An excitatory paraventricular nucleus to
880 AgRP neuron circuit that drives hunger. *Nature* 507, 238–242.

881 Le Tissier, P., Campos, P., Lafont, C., Romanò, N., Hodson, D.J., Mollard, P., 2017. An updated view
882 of hypothalamic-vascular-pituitary unit function and plasticity. *Nat. Rev. Endocrinol.* 13,
883 257–267.

884 Lecoq, J., Savall, J., Vučinić, D., Grewe, B.F., Kim, H., Li, J.Z., Kitch, L.J., Schnitzer, M.J., 2014.
885 Visualizing mammalian brain area interactions by dual-axis two-photon calcium imaging.
886 *Nat. Neurosci.* 17, 1825–1829.

887 Li, Y., Mathis, A., Grewe, B.F., Osterhout, J.A., Ahanonu, B., Schnitzer, M.J., Murthy, V.N., Dulac,
888 C., 2017. Neuronal Representation of Social Information in the Medial Amygdala of Awake
889 Behaving Mice. *Cell* 171, 1176-1190.e17.

890 Liberti, W.A., Perkins, L.N., Leman, D.P., Gardner, T.J., 2017. An open source, wireless capable
891 miniature microscope system. *J. Neural Eng.* 14, 045001.

892 Lin, M.Z., Schnitzer, M.J., 2016. Genetically encoded indicators of neuronal activity. *Nat. Neurosci.*
893 19, 1142–1153.

894 Lobas, M.A., Tao, R., Nagai, J., Kronschräger, M.T., Borden, P.M., Marvin, J.S., Looger, L.L.,
895 Khakh, B.S., 2019. A genetically encoded single-wavelength sensor for imaging cytosolic and
896 cell surface ATP. *Nat. Commun.* 10, 711.

897 Lu, J., Li, C., Singh-Alvarado, J., Zhou, Z.C., Fröhlich, F., Mooney, R., Wang, F., 2018. MIN1PIPE:
898 A Miniscope 1-Photon-Based Calcium Imaging Signal Extraction Pipeline. *Cell Rep.* 23,
899 3673–3684.

900 Mank, M., Santos, A.F., Drenth, S., Mrcic-Flogel, T.D., Hofer, S.B., Stein, V., Hendel, T., Reiff,
901 D.F., Levelt, C., Borst, A., et al., 2008. A genetically encoded calcium indicator for chronic in
902 vivo two-photon imaging. *Nat. Methods* 5, 805–811.

903 Mao, T., O'Connor, D.H., Scheuss, V., Nakai, J., Svoboda, K., 2008. Characterization and subcellular
904 targeting of GCaMP-type genetically-encoded calcium indicators. *PloS One* 3, e1796.

905 Meng, G., Liang, Y., Sarsfield, S., Jiang, W.-C., Lu, R., Dudman, J.T., Aponte, Y., Ji, N., 2019. High-
906 throughput synapse-resolving two-photon fluorescence microendoscopy for deep-brain
907 volumetric imaging in vivo. *eLife* 8.

908 Montagni, E., Resta, F., Conti, E., Scaglione, A., Pasquini, M., Micera, S., Mascaro, A.L.A., Pavone,
909 F.S., 2018. Wide-field imaging of cortical neuronal activity with red-shifted functional
910 indicators during motor task execution. *J. Phys. Appl. Phys.* 52, 074001.

911 Mukamel, E.A., Nimmerjahn, A., Schnitzer, M.J., 2009. Automated analysis of cellular signals from
912 large-scale calcium imaging data. *Neuron* 63, 747–760.

913 Murphy, T.H., Boyd, J.D., Bolaños, F., Vanni, M.P., Silasi, G., Haupt, D., LeDue, J.M., 2016. High-
914 throughput automated home-cage mesoscopic functional imaging of mouse cortex. *Nat.*
915 *Commun.* 7, 11611.

916 Nakai, J., Ohkura, M., Imoto, K., 2001. A high signal-to-noise Ca(2+) probe composed of a single
917 green fluorescent protein. *Nat. Biotechnol.* 19, 137–141.

918 Odaka, H., Arai, S., Inoue, T., Kitaguchi, T., 2014. Genetically-encoded yellow fluorescent cAMP
919 indicator with an expanded dynamic range for dual-color imaging. *PloS One* 9, e100252.

920 Ohkura, M., Matsuzaki, M., Kasai, H., Imoto, K., Nakai, J., 2005. Genetically encoded bright Ca2+
921 probe applicable for dynamic Ca2+ imaging of dendritic spines. *Anal. Chem.* 77, 5861–5869.

922 Ohta, Y., Furuta, T., Nagai, T., Horikawa, K., 2018. Red fluorescent cAMP indicator with increased
923 affinity and expanded dynamic range. *Sci. Rep.* 8, 1866.

924 Ozbay, B.N., Futia, G.L., Ma, M., Bright, V.M., Gopinath, J.T., Hughes, E.G., Restrepo, D., Gibson,
925 E.A., 2018. Three dimensional two-photon brain imaging in freely moving mice using a
926 miniature fiber coupled microscope with active axial-scanning. *Sci. Rep.* 8, 8108.

927 Palmer, A.E., Tsien, R.Y., 2006. Measuring calcium signaling using genetically targetable fluorescent
928 indicators. *Nat. Protoc.* 1, 1057–1065.

929 Patriarchi, T., Cho, J.R., Merten, K., Howe, M.W., Marley, A., Xiong, W.-H., Folk, R.W., Broussard,
930 G.J., Liang, R., Jang, M.J., et al., 2018. Ultrafast neuronal imaging of dopamine dynamics
931 with designed genetically encoded sensors. *Science* 360.

932 Pérez Koldenkova, V., Nagai, T., 2013. Genetically encoded Ca(2+) indicators: properties and
933 evaluation. *Biochim. Biophys. Acta* 1833, 1787–1797.

934 Pinto, L., Dan, Y., 2015. Cell-Type-Specific Activity in Prefrontal Cortex during Goal-Directed
935 Behavior. *Neuron* 87, 437–450.

936 Pnevmatikakis, E.A., 2019. Analysis pipelines for calcium imaging data. *Curr. Opin. Neurobiol.* 55,
937 15–21.

938 Pnevmatikakis, E.A., Giovannucci, A., 2017. NoRMCorre: An online algorithm for piecewise rigid
939 motion correction of calcium imaging data. *J. Neurosci. Methods* 291, 83–94.

940 Pnevmatikakis, E.A., Soudry, D., Gao, Y., Machado, T.A., Merel, J., Pfau, D., Reardon, T., Mu, Y.,
941 Lacefield, C., Yang, W., et al., 2016. Simultaneous Denoising, Deconvolution, and Demixing
942 of Calcium Imaging Data. *Neuron* 89, 285–299.

943 Pomrenze, M.B., Millan, E.Z., Hopf, F.W., Keiflin, R., Maiya, R., Blasio, A., Dadgar, J., Kharazia,
944 V., De Guglielmo, G., Crawford, E., et al., 2015. A Transgenic Rat for Investigating the
945 Anatomy and Function of Corticotrophin Releasing Factor Circuits. *Front. Neurosci.* 9, 487.

946 Remedios, R., Kennedy, A., Zelikowsky, M., Grewe, B.F., Schnitzer, M.J., Anderson, D.J., 2017.
947 Social behaviour shapes hypothalamic neural ensemble representations of conspecific sex.
948 *Nature* 550, 388–392.

949 Resendez, S.L., Jennings, J.H., Ung, R.L., Namboodiri, V.M.K., Zhou, Z.C., Otis, J.M., Nomura, H.,
950 McHenry, J.A., Kosyk, O., Stuber, G.D., 2016. Visualization of cortical, subcortical and deep
951 brain neural circuit dynamics during naturalistic mammalian behavior with head-mounted
952 microscopes and chronically implanted lenses. *Nat. Protoc.* 11, 566–597.

953 Romanov, R.A., Zeisel, A., Bakker, J., Girach, F., Hellyasz, A., Tomer, R., Alpár, A., Mulder, J.,
954 Clotman, F., Keimpema, E., et al., 2017. Molecular interrogation of hypothalamic
955 organization reveals distinct dopamine neuronal subtypes. *Nat. Neurosci.* 20, 176–188.

956 Rungta, R.L., Osmanski, B.-F., Boido, D., Tanter, M., Charpak, S., 2017. Light controls cerebral
957 blood flow in naive animals. *Nat. Commun.* 8, 14191.

958 Saha, J.K., Xia, J., Grondin, J.M., Engle, S.K., Jakubowski, J.A., 2005. Acute hyperglycemia induced
959 by ketamine/xylazine anesthesia in rats: mechanisms and implications for preclinical models.
960 *Exp. Biol. Med.* Maywood NJ 230, 777–784.

961 Sakuma, T., Barry, M.A., Ikeda, Y., 2012. Lentiviral vectors: basic to translational. *Biochem. J.* 443,
962 603–618.

963 Samulski, R.J., Muzyczka, N., 2014. AAV-Mediated Gene Therapy for Research and Therapeutic
964 Purposes. *Annu. Rev. Virol.* 1, 427–451.

965 Scott, B.B., Thiberge, S.Y., Guo, C., Tervo, D.G.R., Brody, C.D., Karpova, A.Y., Tank, D.W., 2018.
966 Imaging Cortical Dynamics in GCaMP Transgenic Rats with a Head-Mounted Widefield
967 Macroscope. *Neuron* 100, 1045-1058.e5.

968 Seutin, V.M., 2003. Mechanisms of actions of inhaled anesthetics. *N. Engl. J. Med.* 349, 909–910;
969 author reply 909-910.

970 Steinmetz, N.A., Buettner, C., Lecoq, J., Lee, C.R., Peters, A.J., Jacobs, E.A.K., Coen, P.,
971 Ollerenshaw, D.R., Valley, M.T., de Vries, S.E.J., et al., 2017. Aberrant Cortical Activity in
972 Multiple GCaMP6-Expressing Transgenic Mouse Lines. *eNeuro* 4.

973 Steyn, F.J., Huang, L., Ngo, S.T., Leong, J.W., Tan, H.Y., Xie, T.Y., Parlow, A.F., Veldhuis, J.D.,
974 Waters, M.J., Chen, C., 2011. Development of a method for the determination of pulsatile
975 growth hormone secretion in mice. *Endocrinology* 152, 3165–3171.

976 Steyn, F.J., Wan, Y., Clarkson, J., Veldhuis, J.D., Herbison, A.E., Chen, C., 2013. Development of a
977 methodology for and assessment of pulsatile luteinizing hormone secretion in juvenile and
978 adult male mice. *Endocrinology* 154, 4939–4945.

979 Tallini, Y.N., Ohkura, M., Choi, B.-R., Ji, G., Imoto, K., Doran, R., Lee, J., Plan, P., Wilson, J., Xin,
980 et al., 2006. Imaging cellular signals in the heart in vivo: Cardiac expression of the high-
981 signal Ca²⁺ indicator GCaMP2. *Proc. Natl. Acad. Sci. U. S. A.* 103, 4753–4758.

982 Thrane, A.S., Rangroo Thrane, V., Zeppenfeld, D., Lou, N., Xu, Q., Nagelhus, E.A., Nedergaard, M.,
983 2012. General anesthesia selectively disrupts astrocyte calcium signaling in the awake mouse
984 cortex. *Proc. Natl. Acad. Sci. U. S. A.* 109, 18974–18979.

985 Vasileva, A., Jessberger, R., 2005. Precise hit: adeno-associated virus in gene targeting. *Nat. Rev.*
986 *Microbiol.* 3, 837–847.

987 Viskaitis, P., Irvine, E.E., Smith, M.A., Choudhury, A.I., Alvarez-Curto, E., Glegola, J.A., Hardy,
988 D.G., Pedroni, S.M.A., Paiva Pessoa, M.R., Fernando, A.B.P., et al., 2017. Modulation of
989 SF1 Neuron Activity Coordinately Regulates Both Feeding Behavior and Associated
990 Emotional States. *Cell Rep.* 21, 3559–3572.

991 Voliotis, M., Li, X.F., De Burgh, R., Lass, G., Lightman, S.L., O’Byrne, K.T., Tsaneva-Atanasova,
992 K., 2019. The Origin of GnRH Pulse Generation: An Integrative Mathematical-Experimental
993 Approach. *J. Neurosci. Off. J. Soc. Neurosci.* 39, 9738–9747.

994 Walker, J.J., Spiga, F., Waite, E., Zhao, Z., Kershaw, Y., Terry, J.R., Lightman, S.L., 2012. The
995 origin of glucocorticoid hormone oscillations. *PLoS Biol.* 10, e1001341.

996 Wang, C., Ma, W., 2019. Hypothalamic and pituitary transcriptome profiling using RNA-sequencing
997 in high-yielding and low-yielding laying hens. *Sci. Rep.* 9, 10285.

998 Windle, R.J., Wood, S.A., Lightman, S.L., Ingram, C.D., 1998. The Pulsatile Characteristics of
999 Hypothalamo-Pituitary-Adrenal Activity in Female Lewis and Fischer 344 Rats and Its
1000 Relationship to Differential Stress Responses. *Endocrinology* 139, 4044–4052.

1001 Yasuda, R., Nimchinsky, E.A., Scheuss, V., Polgruto, T.A., Oertner, T.G., Sabatini, B.L., Svoboda,
1002 K., 2004. Imaging calcium concentration dynamics in small neuronal compartments. *Sci.*
1003 *STKE Signal Transduct. Knowl. Environ.* 2004, pl5.

1004 Zhang, L., Liang, B., Barbera, G., Hawes, S., Zhang, Y., Stump, K., Baum, I., Yang, Y., Li, Y., Lin,
1005 D.-T., 2019. Miniscope GRIN Lens System for Calcium Imaging of Neuronal Activity from
1006 Deep Brain Structures in Behaving Animals. *Curr. Protoc. Neurosci.* 86, e56.

1007 Zhou, P., Resendez, S.L., Rodriguez-Romaguera, J., Jimenez, J.C., Neufeld, S.Q., Giovannucci, A.,
1008 Friedrich, J., Pnevmatikakis, E.A., Stuber, G.D., Hen, R., et al., 2018. Efficient and accurate
1009 extraction of in vivo calcium signals from microendoscopic video data. *eLife* 7.

1010 Zimmerman, C.A., Huey, E.L., Ahn, J.S., Beutler, L.R., Tan, C.L., Kosar, S., Bai, L., Chen, Y.,
1011 Corpuz, T.V., Madisen, L., et al., 2019. A gut-to-brain signal of fluid osmolarity controls
1012 thirst satiation. *Nature* 568, 98–102.

1013 Ziv, Y., Burns, L.D., Cocker, E.D., Hamel, E.O., Ghosh, K.K., Kitch, L.J., El Gamal, A., Schnitzer,
1014 M.J., 2013. Long-term dynamics of CA1 hippocampal place codes. *Nat. Neurosci.* 16, 264–
1015 266.

1016 Zong, W., Wu, R., Li, M., Hu, Y., Li, Y., Li, J., Rong, H., Wu, H., Xu, Y., Lu, Y., et al., 2017. Fast
1017 high-resolution miniature two-photon microscopy for brain imaging in freely behaving mice.
1018 *Nat. Methods* 14, 713–719.

1019

1020

1021
1022
1023
1024
1025
1026

1027 • **Figure Legends:**

1028

1029 **Figure 1: Deep-brain imaging as a powerful tool to understand neuroendocrine functioning.**

1030 Unknowns such as the relationship between the activity of specific neurons and the dynamics of
1031 peripheral hormonal secretion (A), or the way newly discovered genetic mutations result in phenotypic
1032 changes (B) can be elucidated using *in vivo* deep brain imaging (C). Researchers will greatly benefit
1033 from real time visualisation of single neuron calcium activity (D), population calcium activity (E), and
1034 will gain insight into the network activity of genetically defined neurons (F).

1035

1036 **Figure 2: *In vivo* calcium imaging of TRH neurons in conscious mice.**

1037 A. TRH-Cre mice were injected in the median eminence with a viral vector
1038 (AAV5.CAG.Flex.GCaMP6s.WPRE.SV40) . B. Immunofluorescence image showing GCaMP6s
1039 expression (green) in TRH neurons (red). C. GRIN lens view of a field of the TRH neurons expressing
1040 GCaMP6m. Regions of interest corresponding to individual neurons are indicated by coloured arrows.
1041 D. Time-lapse recordings of calcium (GCaMP6s) activity of 8 hypophysiotropic TRH neurons in an
1042 adult TRH-Cre male mouse. Scale bars 50 μ m

1043

1044 **Figure 3: Isoflurane changes the calcium activity of arcuate nucleus neurons.**

1045 25-minute-long *in vivo* recordings of arcuate nucleus neurons were performed in head-fixed mice, mice
1046 were then anaesthetised with isoflurane and the same neurons were recorded for another 25 minutes B.
1047 Time-lapse recordings of calcium (GCaMP6s) activity of 7 arcuate nucleus neurons in an awake adult
1048 C57Bl6 male mouse. C. Time-lapse recordings of calcium activity of the same 7 arcuate nucleus
1049 neurons in the same anaesthetised adult male mouse.

1050

1051

1052 **Table 1: Virus Database for the transfection of hypothalamic neurons.**

1053 Brain area abbreviations: MS: medial septum; rPOA: rostral preoptic area; AHA: anterior
1054 hypothalamus; ARN: arcuate nucleus; PVN: paraventricular nucleus; LH: lateral hypothalamus; RP3V:
1055 rostral periventricular region of the third ventricle; VMH: ventro-medial hypothalamus.

1056 Neuronal identity abbreviations: GnRH: gonadotropin-releasing hormone; GHRH: growth hormone-
1057 releasing hormone; CRH: corticotropin-releasing hormone; TRH: thyrotropin-releasing hormone;
1058 POMC: Pro-opiomelanocortin; AgRP: Agouti-related peptide; GABA: gamma-aminobutyric acid.

1059

1060 **Table 2: Comparison of the characteristics of the Inscopix nVista miniature microscope and**
1061 **UCLA Miniscope.**

1062 * The field of view given for the 3rd generation UCLA Miniscope is based on imaging superficial brain
1063 structures. The addition of an objective GRIN lens that is required to image deep-brain structures
1064 reduces this field of view. To our knowledge, precise field of view measurements for deep brain imaging
1065 using this miniscope are not known.

1066

1067 **Box 1: Typical step-by-step approach toward *in vivo* deep-brain calcium imaging.**

Table 1: Virus database for the transfection of hypothalamic neurons.

Serotype	Promoter	Transgene	Host Specie	Brain area	Neuronal Identity	References
9	EF1a	ChR2	mouse, rat	MS, rPOA, AHA	GnRH	(Campos and Herbison 2014) and unpublished data
9, 5, 2	EF1a, CAG	ChR2, GCaMP6s	mouse	ARN	GHRH	Unpublished data
9, 5, 2	EF1a, CAG	ChR2, GCaMP6s	Mouse, rat	PVN, LH	CRH	(Romanov et al. 2017; Füzesi et al. 2016; Pomrenze et al. 2015)
9, 8, 5, 2	EF1a, CAG, Syn	ChR2, GCaMP6s GCaMP6m, hM3Dq	Mouse	PVN,	TRH	(Krashes et al. 2014) and unpublished data
9	EF1a	ChR2, GCaMP6s, ArchR, HaloR hM3Dq, hM4Di	mouse	RP3V, ARN	Kisspeptin	(Clarkson et al. 2017; Han et al. 2015)
5	CAG	hM4Di	mouse	ARN	POMC	(Atasoy et al. 2012)
1, 8	Syn,	ChR2, ArchR, GCamp6s, hM4Di	mouse	ARN	AgRP	(Atasoy et al. 2012; Betley, Xu, Fang, et al. 2015; Krashes et al. 2014)
1, DJ,9, 5	Syn, Ef1a,	GCamp6s, ChETA, hM3Dq, eYFP	mouse	LH, ARN	GABAergic	(Jennings et al. 2015; Resendez et al. 2016; Silva et al. 2019)
1	Syn	GCamp6s	mouse	VMH	Galanergic	(Viskaitis et al. 2017)
1	Syn	GCamp6s	mouse	VMH	Estrogen receptor 1	(Remedios et al. 2017)

Footnotes:

Brain area abbreviations: MS: medial septum; rPOA: rostral preoptic area; AHA: anterior hypothalamus; ARN: arcuate nucleus; PVN: paraventricular nucleus; LH: lateral hypothalamus; RP3V: rostral periventricular region of the third ventricle; VMH: ventro-medial hypothalamus.

Neuronal identity abbreviations: GnRH: gonadotropin-releasing hormone; GHRH: growth hormone-releasing hormone; CRH: corticotropin-releasing hormone; TRH: thyrotropin-releasing hormone; POMC: Pro-opiomelanocortin; AgRP: Agouti-related peptide; GABA: gamma-aminobutyric acid.

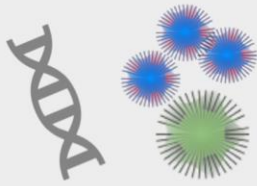
Table 2: Comparison of the characteristics of the Inscopix nVista miniature microscope and UCLA Miniscope.

System	UCLA Miniscope- 3rd generation	nVista 4th generation
Weight (g)	3	1.8
Size L x W x H (mm)	16.3 x 13 x 22.5	8.8 x 15 x 22
Footprint on skull (Baseplate)(mm²)	75	57.44
Resolution (pixels)	752 x 480	1280 x 800
Field of view (µm)	700 x 450 *	650 x 900
Sample-rate (Hz)	60	50
Focusing mechanism	Manual (300 µm) - Slider	Electronic (300 µm) - Liquid lens

Footnote:

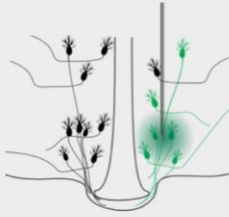
* The field of view given for the 3rd generation UCLA Miniscope is based on imaging superficial brain structures. The addition of an objective GRIN lens that is required to image deep-brain structures reduces this field of view. To our knowledge, precise field of view measurements for deep brain imaging using this miniscope are not known.

Box 1



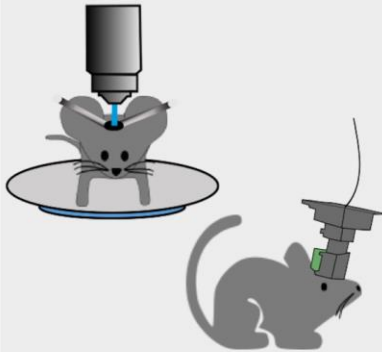
1. Preliminary steps:

- Define which calcium Indicator will be best fitted. AIM for high SNRs.
- Define a strategy to target GECIs to the cells of interest:
- Viral approach: AAVs (most used) vs LVs (large DNA sequences)
- Transgenic approach: conditional knock-in or promoter-specific expression



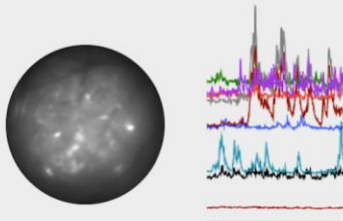
2. Targeting and testing GECIs *ex vivo*:

- Viral approach: Perform stereotaxic surgeries to determine target coordinates, virus volume and concentration and delay for expression
- Viral and transgenic approaches: histological analysis. Nuclear exclusion of GCaMP? Into target cells?
- Ex vivo dual electrical-calcium activity recordings of GCaMP-expressing neurons



3. *In vivo* calcium imaging

- Stereotaxic surgeries: GRIN lens implantation
- Histological and physiological tests after GRIN lens implantation
- Animal handling/habituation
- Head-fixed recordings preferably in a first instance. Better image quality and easier to perform.
- Miniscope building/sourcing
- Chronic long-term in vivo calcium activity recordings
- Control for stress: corticosterone assay
- Experimental paradigm: behavioral tests/blood sampling



4. Calcium activity analysis.

- Requires a powerful analysis computer
- Analysis packages or step by step approach
- Signal filtering, motion correction, registration, spike interference
- Match calcium activity data with behavioral/hormonal data

Figure 1

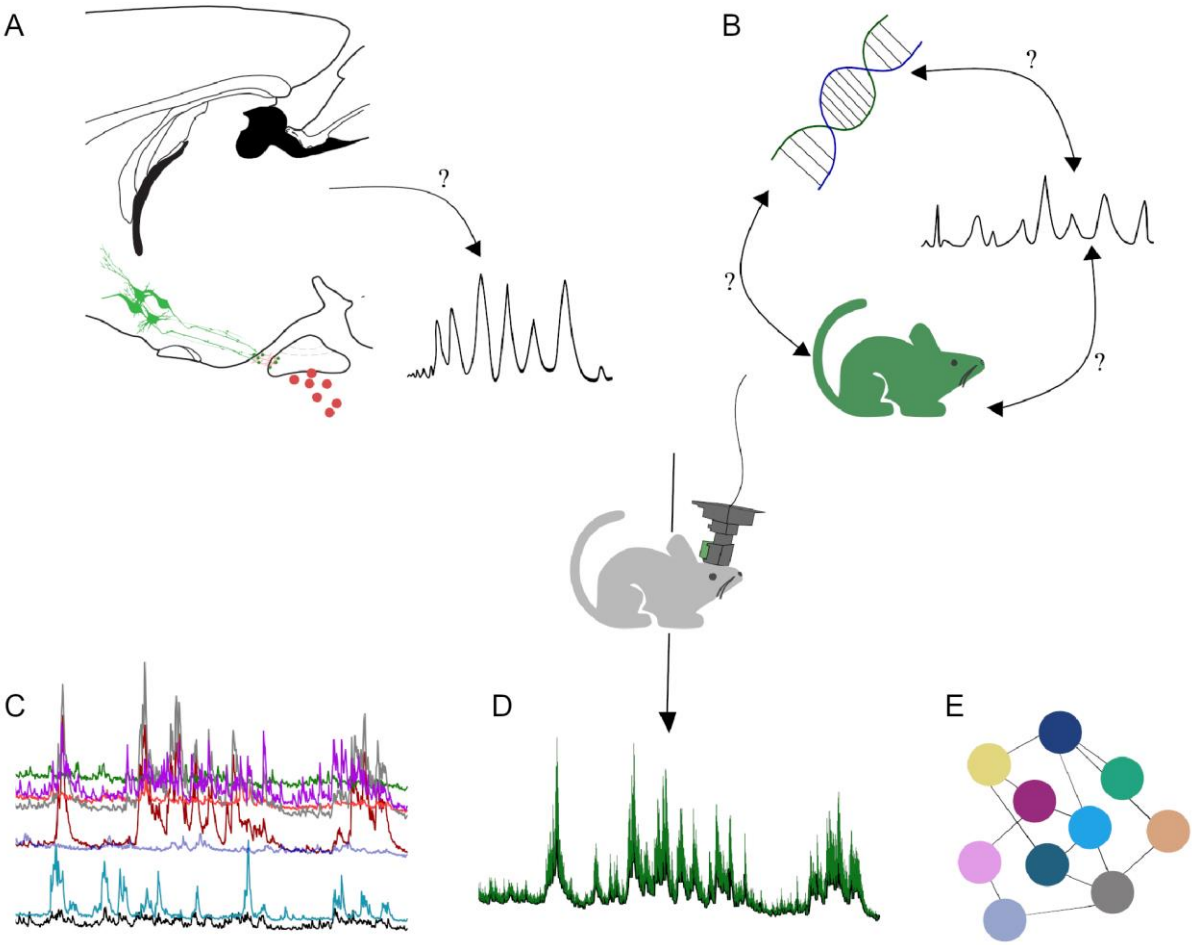


Figure 2

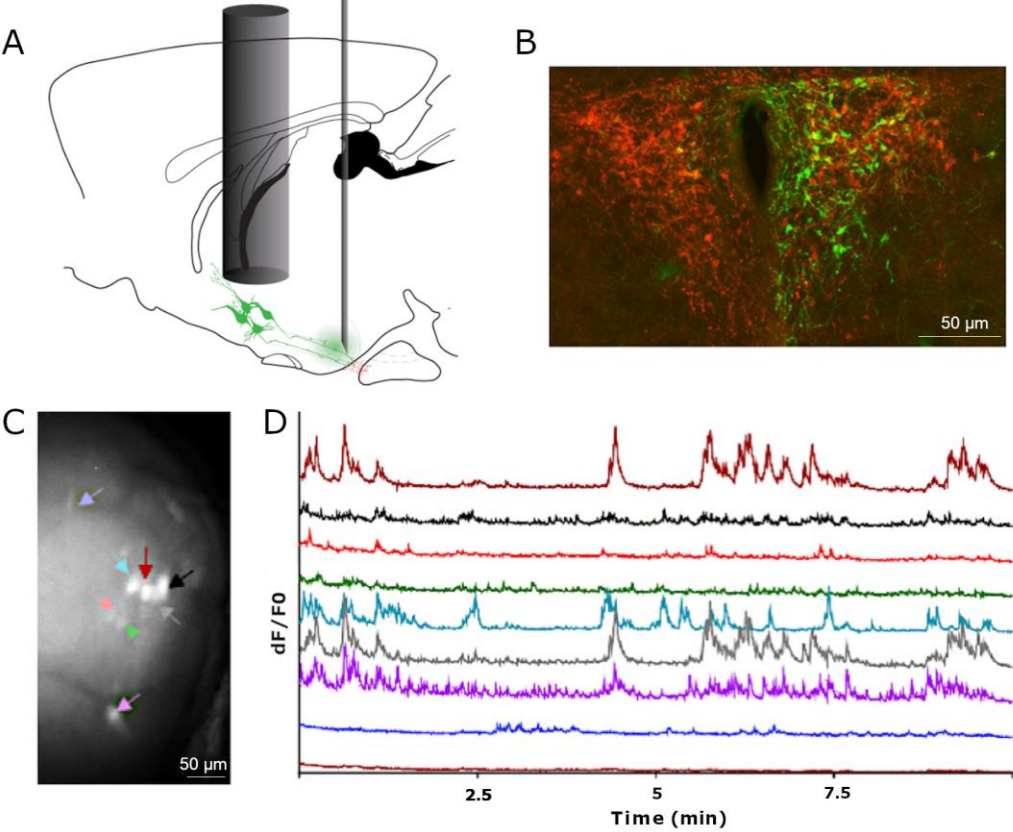


Figure 3:

